

# UNSTEADY FLOW AND ACOUSTIC BEHAVIOUR OF AN AXIAL FAN: NUMERICAL AND EXPERIMENTAL INVESTIGATIONS

*M. Younsi – ANSYS France*

*J. Lavedrine – ANSYS France*

ANSYS France SAS, Montigny Le Bretonneux, France

[mohand.younsi@ansys.com](mailto:mohand.younsi@ansys.com)

[jacques.lavedrine@ansys.com](mailto:jacques.lavedrine@ansys.com)

## ABSTRACT

The purpose of this study is to investigate and qualify the unsteady flow behavior in a complete 6-bladed axial fan and its impact on the noise generation. Computational Fluid Dynamics (CFD) analysis based on the Scale-Adaptive Simulation (SAS) turbulence model has been carried out, taking into account the complex environment of the axial fan.

Additionally, the unsteady variables provided by the numerical simulations have been employed in the Ffowcs-Williams and Hawkings (FW-H) model in order to predict the far field radiated sound at various locations. On the other hand, the numerical results have been compared to the measurement data at the near field.

## NOMENCLATURE

$r$	Radial coordinate	$y^+$	Dimensionless wall distance
$R_{\text{hub}}$	Radius at the hub	$u_0$	Reference velocity
$R_{\text{shroud}}$	Radius at the shroud	$u'$	Turbulent fluctuating velocity
$Re$	Reynolds number	$k$	Turbulent kinetic energy
$Ma$	Mach number	$\bar{U}$	Mean velocity
$N$	Rotation speed	$\bar{U}_a$	Mean axial velocity
$V$	Volumetric flow rate	$\bar{U}_t$	Mean circumferential velocity
$\Delta P$	Static pressure rise	$\bar{U}_r$	Mean radial velocity
$\eta$	Efficiency		

## INTRODUCTION

Axial fans are used in a wide range of industries, ranging from aeronautics and automotive applications to cooling strategies for industrial processes. Computational Fluid Dynamics (CFD) for 3D viscous flow is considered as an efficient tool for analysis, design and optimization particularly in the turbomachinery domain. The unsteady flow description is very important to understand the rotor-stator interactions and their impact on the noise generation. For this reason, there is a continuously increasing demand in turbomachinery area for unsteady flow simulations.

Several researchers have made significant contributions to study unsteady flow and acoustic behavior in fans using different methods. Concerning the use of CFD analysis in this field, Reese et al. (2008) studied a low pressure axial impeller and obtained from CFD analysis the relevant dipole sound sources. The unsteady numerical data were used both in the acoustic analogy model (Ffowcs-

Williams and Hawkings (FW-H)) and the boundary element formulation in order to predict the radiated sound. Younsi et al. (2008) performed a simulation in a centrifugal fan in order to predict the wall pressure fluctuations around a volute casing. In their study, unsteady flow features and noise sources were identified in the near field and compared to experimental data. Besides, Bamberger et al. (2012) used CFD simulations with a Shear Stress Transport (SST) turbulence approach to optimize axial fans with highly swept blades with respect to aerodynamic losses and noise reduction. With their method, the fan efficiency was increased at the design point and the acoustic measurements showed a decrease in sound emission.

Aeroacoustic predictions of a low-subsonic axial fan were studied by Moreau et al. (2012). In their work, three different methods were used and compared with experimental data. The unsteady simulations data provided by the Scale-Adaptive Simulation (SAS) turbulence method were used in the FW-H analogy to predict the sound radiated by the fan.

A recent work from Zhu and Carolus (2013) concerns the experimental and unsteady numerical investigation of the tip clearance noise of an axial fan. In their study, the noise generation mechanisms were studied numerically using SAS approach coupled with FW-H analogy. They conclude that the tip vortex induced pressure fluctuations form the dipole source mechanism of the noise.

The present study is meant to investigate and qualify the unsteady flow behavior in the complete 6-bladed axial fan and its impact on the sound emission. The whole environment of the fan induces complex flow features, which compels to consider the entire regions surrounding the fan. Thus, a grid of 38 million cells is used and the SAS turbulence model is employed in the flow numerical modeling. The details of the numerical methods and strategies are presented in the next sections. The obtained results are compared with the available experimental data found in the literature on the same geometry.

## **FAN FLOW SIMULATION – METHODOLOGY**

The considered fan simulations are based on previous work from Kergourlay et al. (2006) where the unsteady axial fan behavior has been qualified experimentally. In their paper, the experimental setup is fully detailed and thus, only a crude overview of the bench is given hereafter.

### **Experimental Test Rig Description**

Figure 1 is a schematic of the test bench used. The air flows inside the casing through a diaphragm. The air inflow instrumentation is designed to enable controlled air flow rate at and off the best efficiency point (BEP). A perforated plate is located upstream of the fan to ensure uniform flow properties before reaching the fan region. The air then flows through the fan into the atmosphere at ambient conditions. The test bench is built according to the ISO 5801 Standard, (1997).

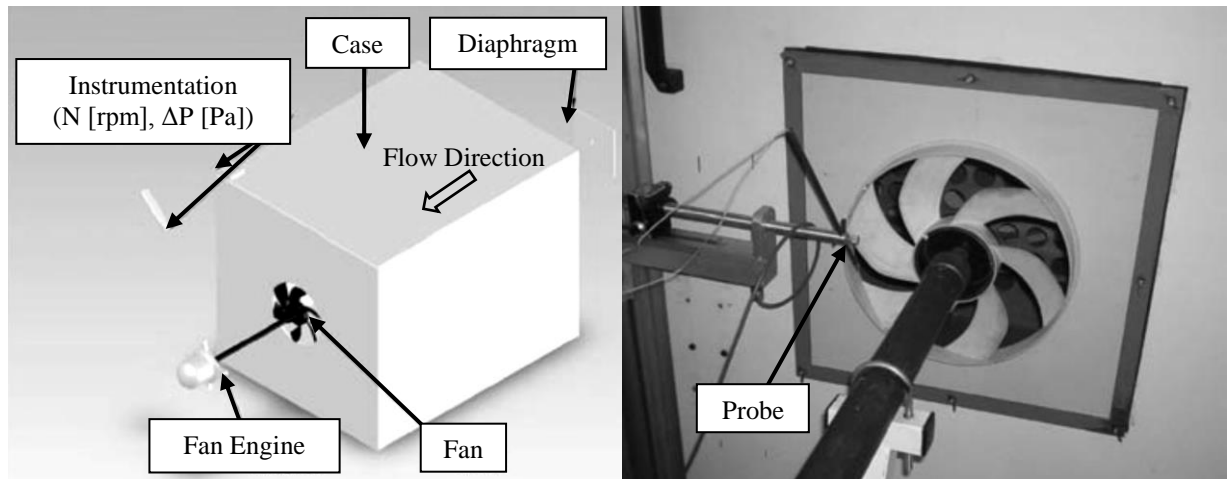


**Figure 1: Sketch of the test bench (left) and Location of the probing device downstream of the fan (right).**

Kergourlay et al. (2006) retained the experimental technique of hot-film constant temperature anemometry. The measurements give access to the unsteady velocity components. They are performed at 11 radial positions downstream of the fan. The hot-wire probe is located 10 mm away from the blade trailing edge, at an angle of  $60^\circ$  to the fan plane, which corresponds to the blowing air direction at the middle span (cf. Figure 1).

The fan is a low-speed axial fan with a forward sweep configuration. The fan includes 6 blades regularly spaced with a hub-to-tip radius ratio ( $R_{\text{hub}} / R_{\text{shroud}}$ ) = 0.38. The studied fan is designed without clearance tip and the blades are rigidly bonded to the shroud (cf. Figure 1). Table 1 gathers the main features of the fan. The operating conditions correspond to the BEP.

FAN CHARACTERISTICS			
Hub Radius $R_{\text{hub}}$	= 0.068 m	Blades count	= 6
Shroud Radius $R_{\text{shroud}}$	= 0.180 m	Rotational Speed $N$	= 2000 rpm
Re ( $R_{\text{shroud}}$ )	= $4.6 \cdot 10^5$	BEP Flow Rate $V$	= $0.63 \text{ m}^3 \text{ s}^{-1}$

**Table 1: Main characteristics of the fan.**

Figure 2 shows the overall fan characteristics such as efficiency and pressure rise.

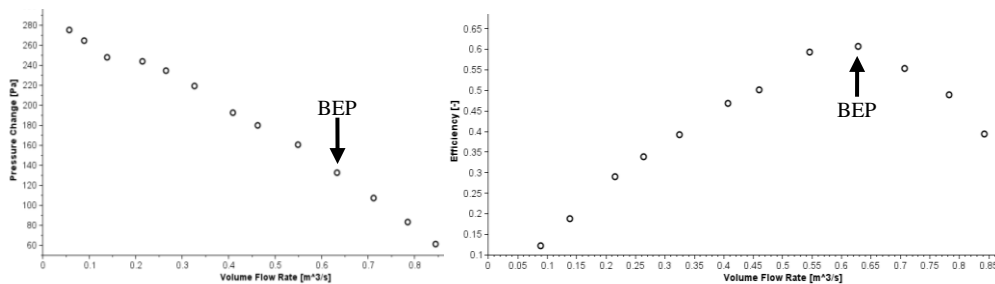


**Figure 2: Fan characteristics vs. volume flow rate: Pressure rise (left), Efficiency (right).**

### Properties of Computational Grid

Figure 3 illustrates the computational domain. In order to reduce computational costs, the casing region was restricted to a smaller fluid volume, enclosing only 25 holes of the perforated plate. The engine axis downstream the fan was also taken into account, so that flow interactions between fan wake and this bench part are correctly modeled. The mesh blocking technique employed in this study is illustrated on a generic blade and has been applied on the actual blade geometry.

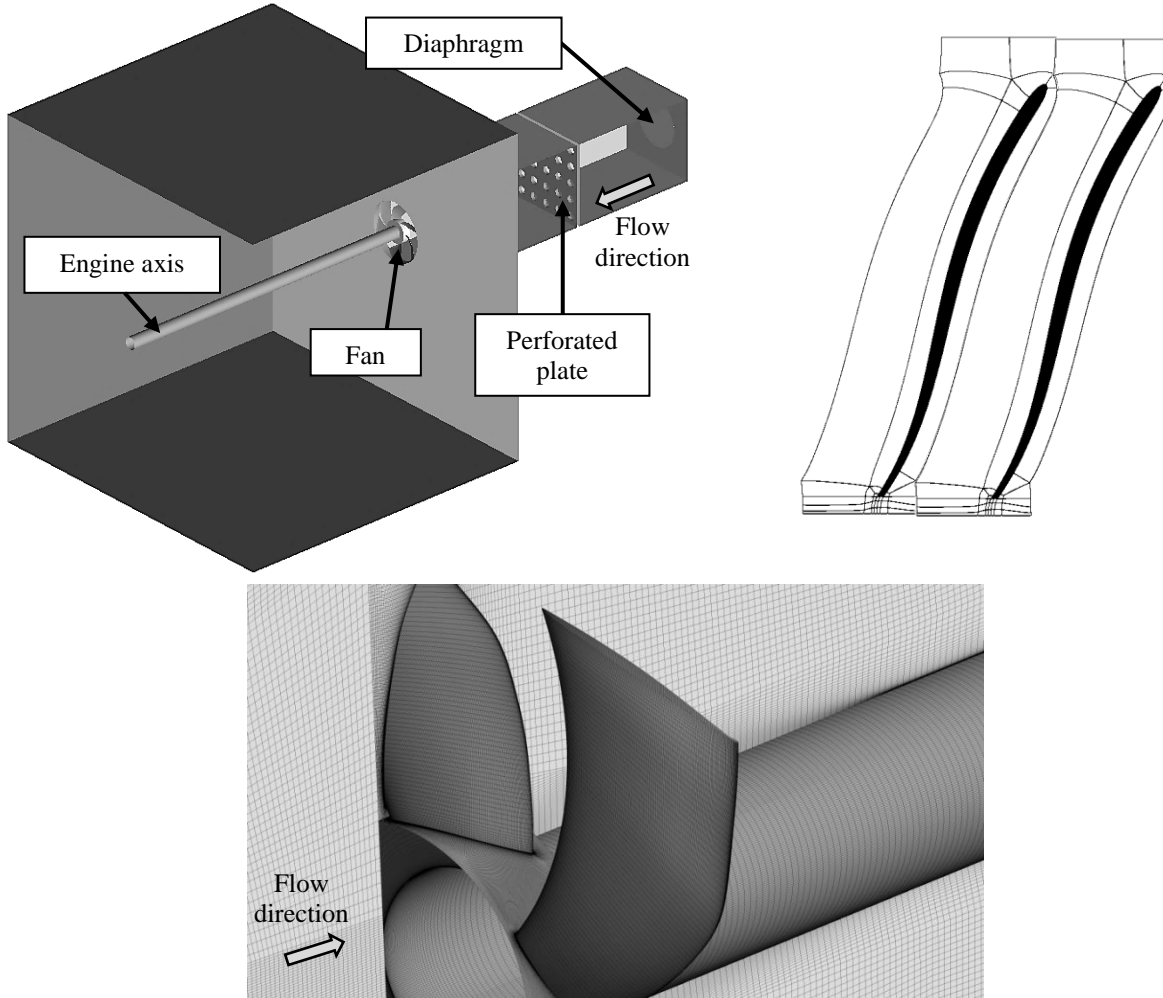


**Figure 3: Overview of the computational domain (top-left), Mesh topology around the blades (top-right) and Details of the grid near the fan (bottom).**

The whole computational grid is split into 3 domains corresponding to the casing, the fan region and the atmosphere. Non-conformal interfaces are used to connect the 3 domains. Sliding mesh technique is used at these interfaces to describe the relative motion between stationary domains and rotating fan. Special attention was devoted to the mesh size distribution across the junctions of the domains.

The near-wall mesh resolution was adapted to the boundary layer flow. The dimensionless wall distance  $y^+$  stands in the range  $[0, 13]$  on the whole domain. Moreover, more than 95% of the grid boundary faces exhibit  $y^+ < 5$ , which allows to solve the boundary layer with the near-wall cell center located in the viscous sub-layer with moderate error. The aspect ratio of cells taken on the blade surface is  $\sim 7$ . A growth ratio of 1.2 in the wall normal direction is necessary to cover the boundary layer with more than 12 cells on fan blades.

Table 2 gathers the main features of the 3 meshed domains. The total number of cells sums up to 38.5 million hexahedra.

Mesh Type	Number of Cells	Mean Cell Size	Min Cell Size	Max( $y^+$ )	% Faces with $y^+ < 5$	Meshing tool
<b>CASE</b>						
Structured	11.0 million	0.004 m	$1.0 \cdot 10^{-5}$ m	$\sim 7$	$\sim 98$	ANSYS ICEM CFD 15.0
<b>FAN</b>						
Structured	8.5 million	0.001 m	$4.0 \cdot 10^{-5}$ m	$\sim 8$	$\sim 98$	ANSYS TurboGrid 15.0
<b>ATMOSPHERE</b>						
Structured	19.0 million	0.004 m	$5.0 \cdot 10^{-5}$ m	$\sim 13$	$\sim 94$	ANSYS ICEM CFD 15.0

**Table 2: Main characteristics of computational grid per domain.**

### **SAS Turbulence Model and Numerical Parameters**

CFD allows to simulate the turbulent flow in the fan via the solution of Navier-Stokes (N-S) equations. However, directly solving N-S equations involves capturing strong non-linear interactions of various-sized eddies in time and space. This statement implies the use of precise high-order numerical schemes, which entails large computational costs. This is the main reason why the Direct Numerical Simulation (DNS) is computationally unaffordable for 3D industrial configurations (Moin and Mahesh, 1998). Thus, the N-S equations are usually solved using two approaches: the Reynolds-Averaged Navier-Stokes (RANS) approach and the Large-Eddy Simulation (LES) approach.

The Reynolds averaging commonly refers to a time averaging where physical quantities are averaged over a sufficiently long time to alleviate the influence of flow turbulent fluctuations on the mean flow. This averaging process gives rise to unclosed terms that are addressed through a turbulence model (Wilcox, 2006). Even if RANS methods have been developed for decades and provide CFD results for a wide range of engineering applications at an affordable cost, they are still submitted to various shortcomings related to the concurrent presence of various-sized turbulent eddies. Such shortcomings are restrictive for turbomachinery flows where complex phenomena such as flow separations and reattachments, vortex shedding and strong free-stream turbulence occur (Tucker et al., 2010b). On the other hand, the LES approach filters the N-S equations based on a grid sizing. This filtering is used to distinguish large (e.g. resolved) eddies from sub-grid scales that require a turbulence closure (Meneveau and Katz, 2000). LES is quite a promising method for turbomachinery applications (Menzies, 2009, Tucker et al., 2010a, Tucker et al., 2010b). However, wall-resolved LES is still very demanding in terms of computational resources: (Chapman, 1979) initially suggested a scaling of approximately  $Re^{1.8}$  and (Choi and Moin, 2011) recently defined a refined scaling of  $Re_{L_x}^{13/7}$  where  $L_x$  is the flat-plate length in the streamwise direction.

In this paper, the SAS model is employed. SAS is a hybrid RANS-LES approach. This model provides a weakly unsteady state solution in stable flow regions such as boundary layers, and populates a wider turbulent spectrum of large unsteady structures in unsteady zones (Menter and Egorov, 2010). SAS includes higher derivatives of the velocity that allow the model to adapt to the resolved turbulent eddies without introducing large dissipation levels as observed in pure RANS approaches. SAS copes with the transition between RANS and LES modes within a single model framework, which is the main difference with Detached-Eddy Simulations (DES) where a separation region must be explicitly defined in the model (Spalart et al., 1997, Squires, 2003). First DES studies showed limitations due to cell size affecting eddy viscosity in boundary layers and more advanced methods like delayed DES (DDES) emerged to tackle this disturbing phenomenon called grid-induced separation (GIS) (Spalart, 2009). In fact, DDES length-scale limiter relies on the solution, rather than on the grid sizing solely, thus automatically prolonging RANS mode in boundary layers (Spalart, 2009).

The unsteady simulation of the turbulent flow was conducted with the CFD commercial software ANSYS FLUENT 15. The calculation was initialized with a potential flow in the computational domain. Regarding boundary conditions, at the inlet diaphragm, a mass flow rate of  $0.745 \text{ kg s}^{-1}$  allows to recover the design flow rate (see Table 1). At the outlet, the static pressure is set to ambient conditions, which refers to a relative pressure of 0 Pa. No-slip walls are set everywhere else, except on the casing sides where symmetry conditions are used. The solver uses the upwind 2<sup>nd</sup> order discretization scheme in space and the implicit 2<sup>nd</sup> order discretization in time for all variables. Time step is set to  $1.0 \cdot 10^{-5} \text{ s}$ , allowing CFL number  $< 3$  in the whole domain. This time step corresponds to a fan rotation of 0.12 degrees. No investigations were carried out regarding the influence of the time step. The chosen time step is a compromise between the target CFL value and a reasonable computational effort. The air flow is modeled as an incompressible flow, which seems relevant when considering that Mach number  $\text{Ma} < 0.1$ . Convergence within each time step is reached when residuals with respect to mass, momentum and turbulence quantities decrease by more than 3 orders of magnitude. Flow field quantities are also monitored at relevant locations in order to ensure reasonable flow stabilization.

## FAN FLOW SIMULATION – RESULTS

### Numerical Results of the Turbulent Flow

The experimental data give access to the performance characteristics of the fan. Table 3 compares the experimental and numerical results of the static pressure rise and efficiency at the design flow rate. The difference between simulation and experimental data remains less than +5% on efficiency and around +1% for static pressure rise through the fan, which proves that overall behavior is properly captured by the calculation.

FAN PERFORMANCE	EXPERIMENT	SIMULATION
Efficiency $\eta$	0.60	0.57
Static pressure jump $\Delta P$	132 Pa	133.5 Pa

**Table 3: Comparison of experimental and numerical results on the performance characteristics of the fan.**

Figure 4 shows the iso-surface of the instantaneous  $Q$  invariant (Hussain and Jeong, 1995) colored by the eddy-to-molecular viscosity ratio near the perforated plate.

Flow through plate orifices produces and convects downstream rolling vortices on the jet edges. Eddy-to-viscosity ratios are very low when considering flow eddies near the plate holes. These large-scale transient vortices are then rapidly stretched, bended and eventually dissipated downstream the orifices. This observation can also be related to eddy viscosity levels that increase over 200 times the molecular viscosity for the farthest vorticity structures. On Figure 4, dashed line also marks the end of the detected eddies and roughly corresponds to an axial extent of 20% of the secondary part of the case (cf. Figure 3). Thus, the CFD simulation shows that large-scale structures vanish before reaching the fan stage. The perforated plate homogenizes and straightens the flow downstream. Besides, levels of turbulent intensity obtained in the calculation are rapidly decreasing, passing from 25% near the plate to less than 5% near the fan.

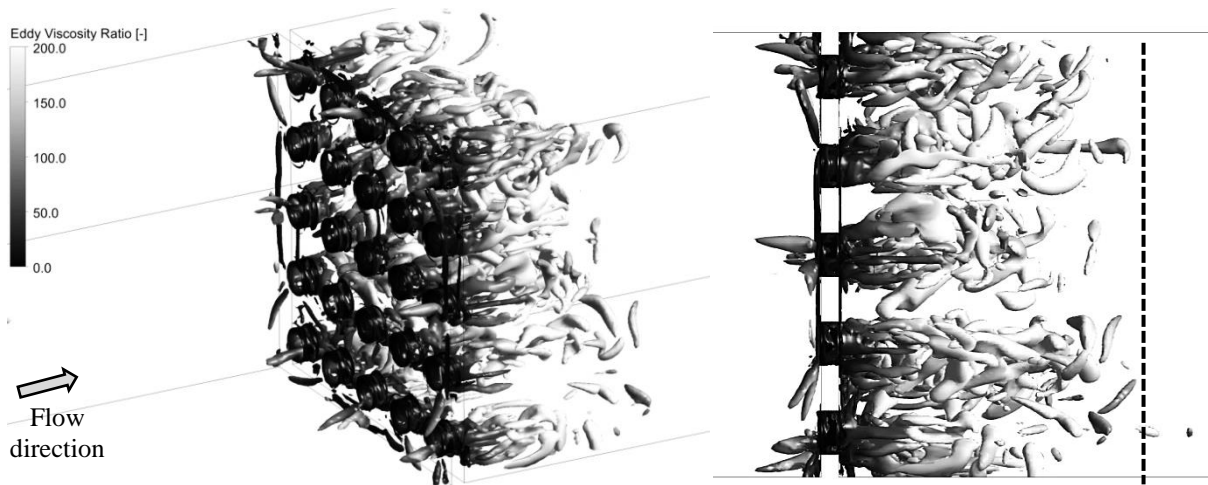


**Figure 4: Perforated plate – Iso-surface of instantaneous  $Q$  invariant colored by the eddy-to-molecular viscosity ratio in isometric view (left) and transverse view (right).**

Figure 5 shows the iso-surface of instantaneous  $Q$  invariant colored by the eddy-to-molecular viscosity ratio near the fan blades and in the fan wake.

The fan blades generate a wide range of unsteady eddies that interact in both circumferential and axial directions. Small eddies are mainly generated near the fan hub and shroud where complex vortex interactions take place. The eddy-viscosity ratio remains low for structures created near the blades and increases in the fan wake. This observation points out that SAS adapts its dissipation level to mesh resolution. Indeed, the turbulent model compensates for the non-resolved eddies in the fan wake.

Thus, the refined structured grid in the fan region allows to capture small eddies in the SAS turbulent approach. Eddies are then convected downstream of the fan, grow in size and extend well beyond the radial level of the shroud. This observation is clearly due to the centrifugal acceleration induced by the fan rotation. In addition to this, the local coarsening of the mesh close to the fan combined with the large blade spacing contribute to enlarging the initial captured eddies. However, these results allow to understand the unsteady flow behavior and the related noise generation mechanisms.

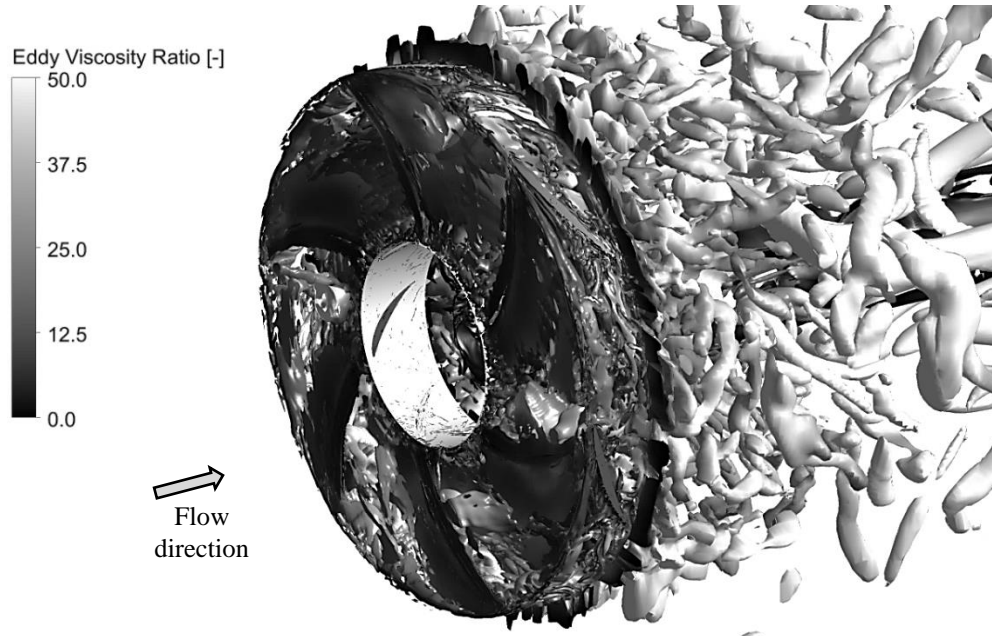


**Figure 5: Fan - Isosurface of instantaneous  $Q$  invariant colored by the eddy-to-molecular viscosity ratio.**

In order to pursue the flow analysis, numerical results are averaged over 3 fan rotation periods to extract mean and fluctuating features of the flow. The averaging process was launched after reaching the stability for unsteady statistical variables.

Figure 6 illustrates the mean velocity and pressure fields in the fan. Regarding the velocity field at the frontal view located at the middle of the fan axial extent, a strong wake can be observed at the blades periphery. Besides, large mean velocity gradients are observed at mid span. This behavior was also reported in Kergourlay et al. (2006). Additionally, the velocity contours show a similar pattern in-between the 6 blades. At design flow rate, no separation of boundary layer at the leading edge is observed in the simulation, which is an expected phenomenon of the flow.

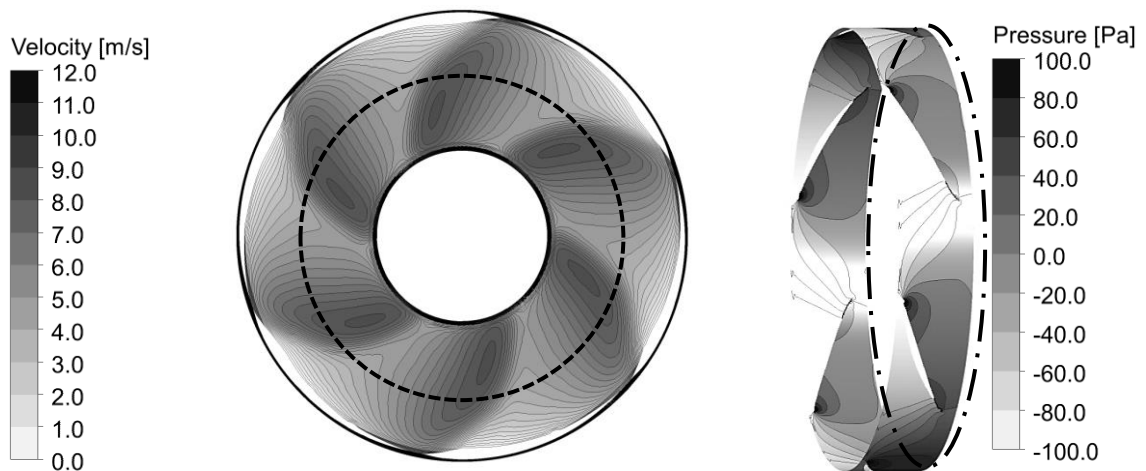


**Figure 6: Fan – Axial cut at the measurements plane (dot-dashed line) colored by the mean velocity (left) and Radial cut at mid span (dashed line) colored by the mean static pressure (right).**

### Comparison between Numerical and Experimental Data

Figure 7 shows the locations of the extracted radial profiles. Experimental data cover only the closest profiles, namely 10 mm downstream of the fan.

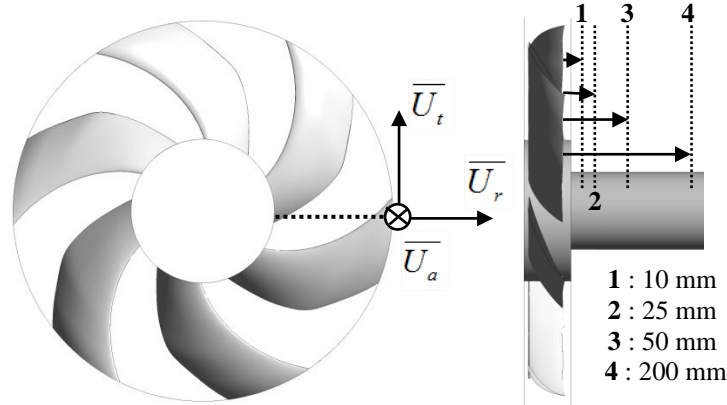


**Figure 7: Fan – Location of radial profiles extracted. Distances are defined starting from the axial level of blade trailing edge.**

The comparison between numerical and experimental data concerns only the available results provided by Kergourlay et al. (2006). Figure 8 gathers the radial profiles of the 3 components of velocity (axial component  $\overline{U}_a$ , circumferential component  $\overline{U}_t$  and radial component  $\overline{U}_r$ ).

Some discrepancies can be observed between experimental and numerical profiles. These discrepancies could be explained by:

- the measurements errors related to :
  - the probing device which modifies locally the unsteady flow,
  - the uncertainties of the bench setup.
- the errors in the numerics which are mainly related to:
  - the grid refinement,
  - the geometry modeling which is not taking into account the hot wire probe.

The axial velocity component shows strong variations with radius in both experiment and calculation. At 10mm downstream of the fan, a high portion of the fan flow passes near the periphery of the fan. Indeed, the maximum air velocity is observed at 80% of  $R_{\text{shroud}}$ . Further cuts extracted from the calculation reveal that the radial profile of the mean axial velocity evolves to a linear form: at 200mm downstream of the fan, the axial velocity becomes directly proportional to radius for  $r < R_{\text{shroud}}$ .

Regarding the other velocity components, numerical results show a reasonable agreement at 10mm downstream of the fan, except for radius near the hub and the shroud where the mean circumferential velocity is underestimated in the calculation. On the one hand, the differences observed in the mean circumferential velocity component are linked to the points listed above. On

the other hand, the short averaging time heavily influences the precision of the velocity profiles. A longer averaging time should most certainly improve this comparison and will be considered in future works. Besides, this local lack of mean circumferential velocity is also reported on the fluctuating kinetic energy  $k$ . The calculated  $k$  shows a shift on the observed peak at the fan periphery: the numerical peak of  $k$  is located at 70% of  $R_{\text{shroud}}$  whereas the experiment shows it at  $R_{\text{shroud}}$ . Close levels of  $k$  are observed in both computational and experimental results, with a maximum at  $9 \text{ m}^2 \text{ s}^{-2}$ .

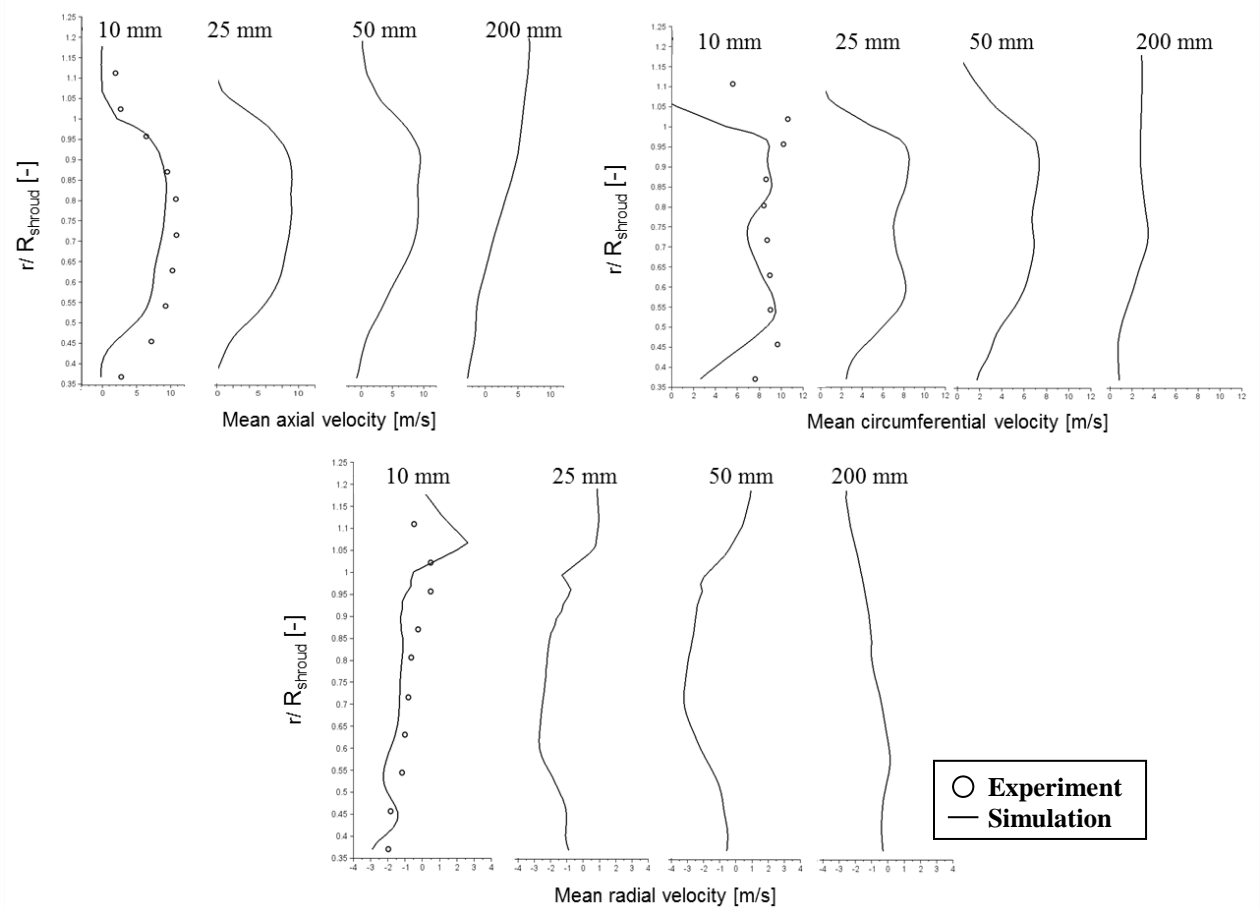


**Figure 8: Fan – Radial profiles of the 3 components of mean velocity.**

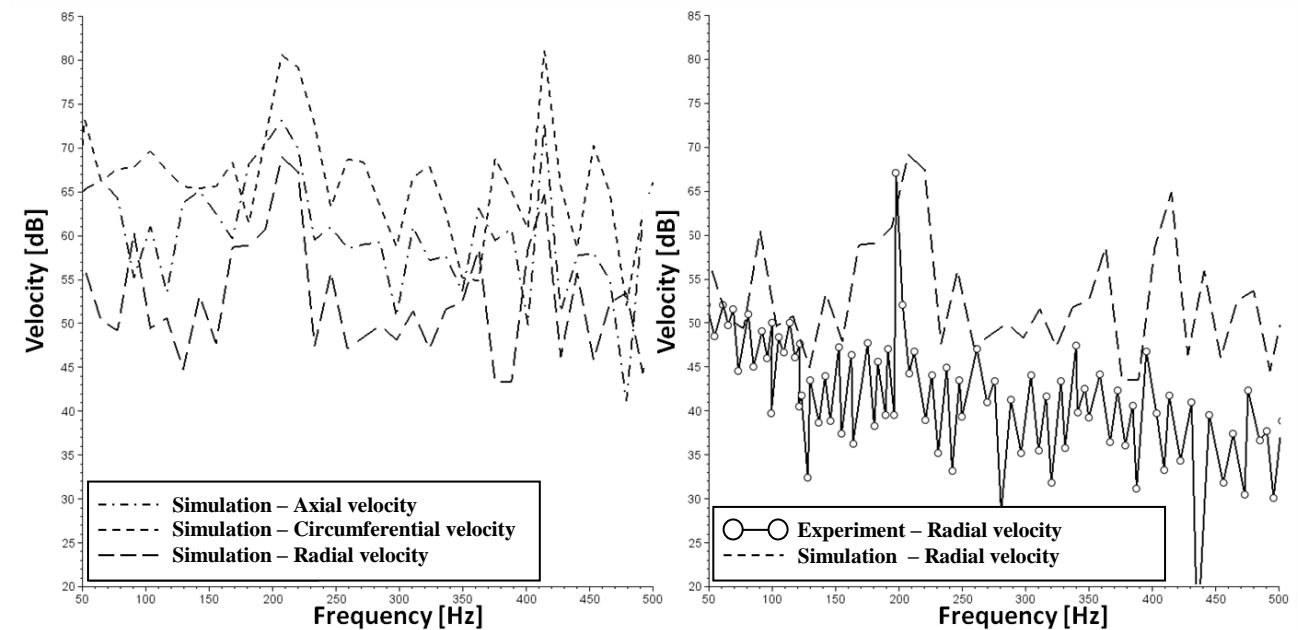
### Spectral Analysis of the Turbulent Flow

Fast Fourier Transform (FFT) data are compared between the experiment and the simulation for the probe located at  $r/R_{\text{shroud}} = 0.87$  and 10mm from the trailing edge. Figure 9 illustrates the spectra plotted in dB on the frequency range 50-500 Hz. The expression  $20 \cdot \log_{10} |u/u_0|$  was used to compute the signal levels where  $u_0$  is a reference velocity equal to 1 m/s.

The near-field velocity spectra show an acceptable agreement between experimental data and numerical results based on radial velocity. The Blade Passing Frequency (BPF) of 200 Hz and its first harmonic at 400 Hz are retrieved in the simulation. Besides, spectra based on other velocity components show the same peaks and higher levels in decibels, which corresponds to larger velocity amplitudes for the axial and circumferential components compared to the radial one.

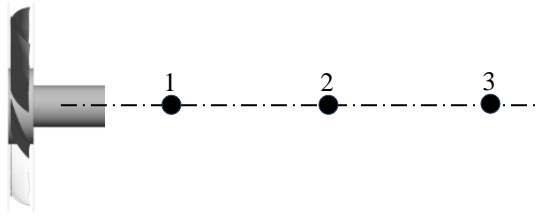
This FFT analysis is carried out on temporal signals obtained during only three fan revolutions which correspond to 0.09 seconds. This duration induces a spectral resolution of 5.5 Hz. This value is obviously greater than the experimental one and explains that the numerical spectra are coarse. A

longer duration of data acquisition will certainly improve these discrepancies, particularly at low frequencies. Future work will allow to further investigate this point (cf. prospects in conclusion section.). In addition to this discussion, the effect of the mesh resolution close to the fan blades could explain the errors in the spectra just after the BPF component. Indeed, the local coarsening of the mesh has a dire impact on adequately capturing the turbulence structures.



**Figure 9: Fan - Spectra of SAS instantaneous velocity components at  $r/R_{\text{shroud}} = 0.87$  (left) and Spectra of instantaneous radial velocity in experiment and SAS simulation (right).**

In order to understand the acoustic behavior of the axial fan, the unsteady flow variables provided by the SAS calculations were used in the FW-H formulation (Williams J.E.F et al., 1969). After reaching the stability for statistical variables, the acquisition of unsteady signals was carried out during 3 fan revolutions. Three receivers were considered to compute the Sound Pressure Level (SPL) at the BPF. The far field receivers 1, 2 and 3 are located on the fan axis respectively at 1, 2 and 3 meters from the fan trailing edge. Table 4 gives the acoustic results at the considered locations and a sound attenuation of 10 dB can be observed with respect to the distance from the fan.

Receiver number	SPL at BPF [dB]	
1	68 dB	
2	61 dB	
3	58 dB	

**Table 4: Sound pressure levels at 3 receivers downstream the fan.**

## CONCLUSIONS AND PROSPECTS

Unsteady flow through axial fan has been studied using SAS turbulence approach in this work. The numerical procedure has been compared locally and globally to available experimental

data obtained in the literature on the same geometry. The complete environment of the fan has been taken into account in order to consider the interaction of the unsteady flow structures generated through the different parts of the test rig. An overall good agreement has been observed between numerical and experimental results.

It should be interesting to extend this study in the future by:

- Increasing the duration of data acquisition with a finer mesh.
- Unsteady post-processing in order to have more details on the near-field unsteadiness and the related signals both in the temporal and frequency domains.
- Spectral analysis at the far field to get a complete acoustic spectrum and additional information on sound directivity.
- More experimental investigations including pressure fluctuations on the blades surfaces,
- Acoustic measurements at the far field in an anechoic room to avoid sound reflections and comparing them to the free-field acoustic analogy.

## ACKNOWLEDGEMENTS

The authors wish to thank:

- Mr. Olivier Ménard from DGA Techniques Hydrodynamiques for his precious help running and analyzing the numerical simulations performed on DGA computational resources.
- Prof. Farid Bakir from DynFluid (Arts et Métiers) for providing the fan geometry.
- Dr. Gérald Kergourlay for his support during the exploitation of experimental data.

## REFERENCES

- Bamberger, K., Carolus, T. (2012): *Optimization of axial fans with highly swept blades with respect to losses and noise reduction*. Fan 2012, Senlis, France.
- Chapman, D. (1979): *Computational aerodynamics development and outlook*. AIAA Journal, Vol. 17, Issue 12, pp. 1293-1313.
- Choi, H., Moin, P. (2011): *Grid-point requirements for large eddy simulation: Chapman's estimates revisited*. Center for Turbulence Research, Annual Research Briefs 2011, pp. 31-36.
- Hussain, F., Jeong, J. (1995): *On the identification of a vortex*. Journal of Fluid Mechanics, Vol. 285, pp. 69-94.
- ISO 5801 (1997): *Industrial fans—performance testing using standardized airways*.
- Kergourlay, G., Kouidri, S., Rankin, G. W., Rey, R. (2006): *Experimental investigation of the 3D unsteady flow field downstream of axial fans*. Flow measurements and instrumentation, Vol. 17, pp. 303-314.
- Meneveau, C., Katz, J. (2000): *Scale-invariance and turbulence models for large eddy simulation*. Annual Review of Fluid Mechanics, Vol. 32, pp. 1-32.
- Menter, F., Egorov, Y. (2010): *The Scale-Adaptive simulation method for unsteady turbulent flow predictions. Part 1: Theory and model description*. Journal of Flow Turbulence and Combustion, Vol. 85, Issue 1, pp. 113-138.
- Menzies, K. (2009): *Large eddy simulation applications in gas turbines*. Philosophical Transactions of the Royal Society, Vol. A367, pp. 2827-2838.
- Moin, P., Mahesh, K. (1998): *Direct numerical simulation: a tool in turbulence research*. Annual Review of Fluid Mechanics, Vol. 30, pp. 539-578.
- Moreau, S., Sanjosé, M., Magne, S., Henner, M. (2012): *Aeroacoustic prediction of a low-subsonic axial fan*. ISROMAC 14, Honolulu, Hawaii, USA.

- Reese, H., Carolus, T. (2008): *Axial fan noise: towards sound prediction based on numerical unsteady flow data – a case study*. Acoustics 08, Paris, France.
- Spalart, P. R., Jou, W. H., Strelets, M., Allmaras, S. R. (1997): *Comments on the feasibility of LES for wings, and on a hybrid RANS/LES approach*. 1st AFOSR International Conference on DNS/LES, Ruston, Louisiana, USA.
- Spalart, P.R. (2009): *Detached-Eddy Simulation*. Annual Review of Fluid Mechanics, Vol. 41, pp. 181-202.
- Squires, K. D. (2003): *Detached-Eddy simulation: Current status and perspectives*. 5<sup>th</sup> International ERCOFTAC Workshop on Direct and Large-Eddy Simulation, Munich, Germany.
- Tucker, P., Eastwood, S., Klostermeier, C., Xia, H., Ray, P., Tyacke, J., Dawes, W. (2010): *Hybrid LES approach for practical turbomachinery flows: Part 1 – Hierarchy and example simulations*. ASME Turbo Expo 2010, Glasgow, UK.
- Tucker, P., Eastwood, S., Klostermeier, C., Xia, H., Ray, P., Tyacke, J., Dawes, W. (2010): *Hybrid LES approach for practical turbomachinery flows: Part 2 – Further applications*. ASME Turbo Expo 2010, Glasgow, UK.
- Williams, J. E. F. and Hawkins, D. L. (1969): *Sound generation by turbulence and surfaces in arbitrary motion*. Philosophical Transactions of the Royal Society, Vol. A264, pp. 321-342.
- Wilcox, D. C. (2006): *Turbulence Modeling for CFD*, DCW Industries, Inc.
- Younsi, M., Djerrada, A., Belamri, T., Menter, F. (2008): *Application of the SAS turbulence model to predict the unsteady flow field behaviour in a forward centrifugal fan*. International Journal of Computational Fluid Dynamics, Vol. 22, Issue 9, pp. 639-648.
- Zhu, T., Carolus, T. H. (2013): *Experimental and Unsteady Numerical Investigation of the Tip Clearance Noise of an Axial Fan*. ASME 2013 Turbine Blade Tip Symposium & Course Week, Hamburg, Germany.